

We are IntechOpen, the world's leading publisher of Open Access books Built by scientists, for scientists

6,100

Open access books available

167,000

International authors and editors

185M

Downloads

Our authors are among the

154

Countries delivered to

TOP 1%

most cited scientists

12.2%

Contributors from top 500 universities



WEB OF SCIENCE™

Selection of our books indexed in the Book Citation Index
in Web of Science™ Core Collection (BKCI)

Interested in publishing with us?
Contact book.department@intechopen.com

Numbers displayed above are based on latest data collected.
For more information visit www.intechopen.com



Chapter

Chiroptical Studies on Anisotropic Condensed Matter: Principle and Recent Applications of the Generalized-High Accuracy Universal Polarimeter

Toru Asahi, Masahito Tanaka, Kenta Nakagawa, Yukana Terasawa, Kazuhiko Ishikawa, Akifumi Takanabe, Hideko Koshima and Bart Kahr

Abstract

Chiroptics is the study of the changes in circular polarization states of light transmitted through analytes typically dissolved in isotropic solutions. However, experimental challenges have long prevented chiroptical measurements of anisotropic media such as single crystals of low symmetry, liquid crystals, or structured films. The high accuracy universal polarimeter (HAUP) was introduced in 1983 to investigate the differential refraction of left and right circular polarization states, circular birefringence (CB), and even in anisotropic media that are dominated by the differential refraction of orthogonal linear polarization states, linear birefringence (LB). In this century, the HAUP was extended to also measure not only the dispersive optical effects (CB and LB) but also the corresponding dissipative effects, circular dichroism (CD) and linear dichroism (LD), differences in light absorption. The improved device is the generalized-HAUP (G-HAUP). Not only can it deliver all the linear optical properties of dissymmetric, anisotropic, and absorbing media, but it can also do so in the ultraviolet as well as the visible part of the electromagnetic spectrum. In this review, characteristic features of the G-HAUP and its applications to crystals of photomechanical salicylidenephenylethylamines, alanine, benzil, and magneto-optical CeF_3 are described.

Keywords: chiroptical properties, circular birefringence, optical activity, circular dichroism, linear birefringence, linear dichroism, chirality, high accuracy universal polarimeter (HAUP), generalized-HAUP (G-HAUP)

1. Introduction

Chiroptics is the study of the transmission of circularly polarized light through transparent analytes. Linear chiroptical effects are circular birefringence (CB), more colloquially known as optical rotation (OR) or optical activity (OA), sometimes described by gyration of magneto-optical tensors, and circular dichroism (CD). Besides the proliferation of near-synonymous terms, *chiroptics* is itself a misnomer. While chirality is a necessary condition for measurement of CB and CD of molecules rapidly, randomly reorienting in isotropic media, chirality is not necessary when measurements are extended to anisotropic media such as single crystals. Molecules in solution must be chiral, characterized by a pure rotational group (C_n , D_n , T , O , I), to be optically active, but some achiral crystals can also be optically active in some directions, in particular those belonging to non-enantiomorphous crystallographic point groups (C_s , C_{2v} , S_4 , D_{2d}) [1]. Thus, the *chiro* prefix is a linguistic infelicity that arose from the historical difficulty of measuring CB and CD in low symmetry crystals, dominated as they are by LB and LD, which can typically be 10^2 – 10^4 times larger than the former. Molecules are small compared with the wavelength of radiation used in spectropolarimetric measurements; thus, CB and CD are small; molecules of 1–2 nm barely feel the sense of the twist of the electric field of circularly polarized light with a pitch of *ca.* 500 nm. By comparison, it is easy to detect small changes in polarization in isotropic media in normal incidence, which are otherwise indifferent to linearly polarized light. However, in solids with much larger competing perturbations to the state of polarization, chiroptical effects can fall within the experimental noise.

OA was evidenced by Arago in 1811 when he passed linearly polarized light along the high-symmetry *c*-axis of quartz [2]. However, the determination of the anisotropy of OA by making off-axis measurements was a challenging area of research as late as 1988 [3]. The minor dissymmetry-induced perturbations to the polarization state of light in anisotropic media is of the same order of magnitude as parasitic ellipticities from imperfect samples and the polarimeter optical components. Consequently, we know comparatively little about the orientational dependence of CB in molecules, a considerable hole in the science of molecular chirality. A strategy for filling this hole is to characterize the chiroptical properties and to understand what responses contribute to the orientational averages measured in solution.

The *intensity* of light passing through a polarizer, chiral anisotropic sample, and analyzer, contains all the necessary information, in principle, for extracting CB even in the presence of dominating LB. However, the implementation of this extraction was only achieved after the invention of electrophotometry and stable, high-intensity light sources. In 1983, Kobayashi and Uesu used photon-counting techniques, lasers, and computerized modulation of polarizer and the analyzer orientations (θ and γ ; see **Figure 1a**) to determine OA in crystals for directions off the optic axes. This so-called HAUP (high accuracy universal polarimeter) [4–6] was a watershed that gave researchers some confidence after almost two centuries that OA could be measured in crystals generally.

Curiously, the acronym *HAUP* itself is also a slight misnomer. While the HAUP was *universal* in tackling circular and linear anisotropies simultaneously, it could not be considered truly universal until it could function as a complete polarimeter, thus delivering CD and LD as well. For this reason, the extended HAUP method and its associated optical analysis were developed to deliver all four optical effects simultaneously: CB, LB, CD, and LD [6, 7]. Moreover, generalized-HAUP (G-HAUP) has now been extended into the ultraviolet part of the electromagnetic spectrum [8].

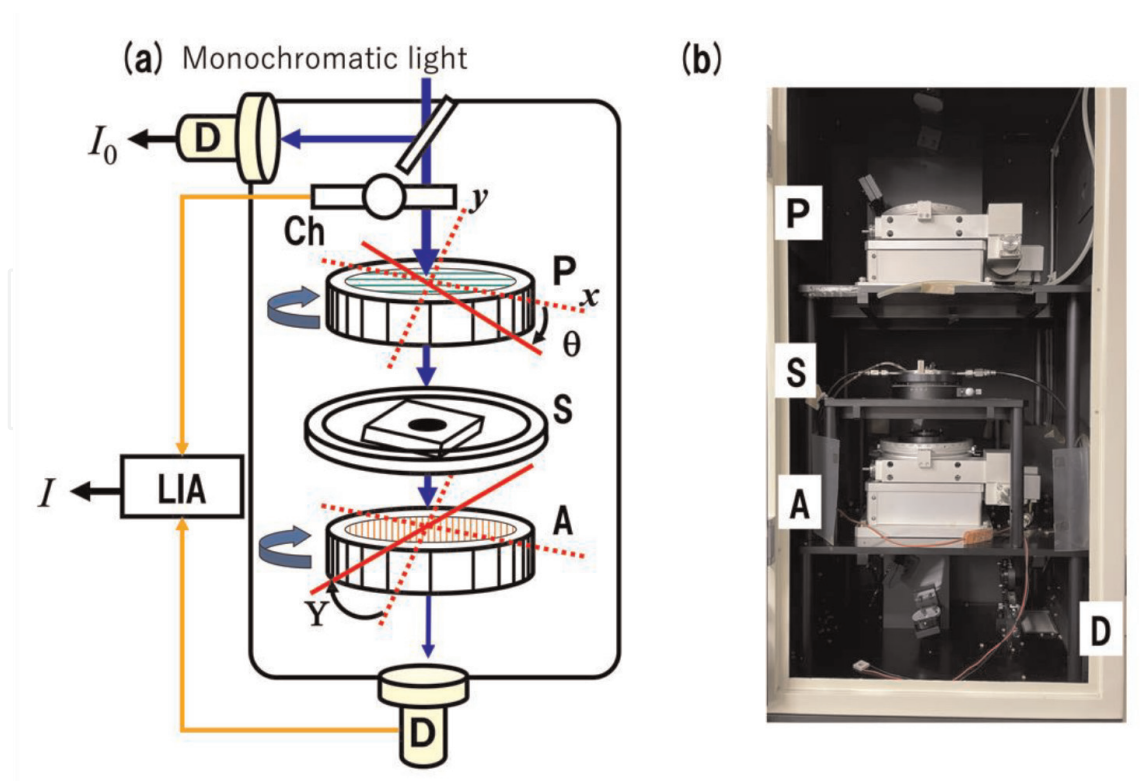


Figure 1.
 (a) Schematic representation of the conventional HAUP optics with optical chopper (Ch), lock-in amplifier (LIA), linear polarizer (P), sample stage with a temperature control unit and a pinhole (S), linear analyzer (A), and detector (D). θ and γ are the azimuth angle of P from an extinction position of a crystalline sample and the deflecting angle α from the crossed Nicols position, respectively. (b) Photograph of the G-HAUP apparatus developed by authors.

In addition to the HAUP [4–9], other strategies have arisen to measure CB and CD in crystals using modulation of light polarization states photoelastically. These include universal chiroptical spectrophotometer (UCS) [10] and the 4 photo-elastic modulator (4PEM) polarimeter [11]. The UCS relies on the fact that the contributions to a time-varying intensity signal have different frequency dependencies and can be isolated with lock-in amplifiers. 4PEM is a complete polarimeter configured to deliver the whole polarization transfer or Mueller matrix and without any moving optical components to minimize errors. In the 4-PEM polarimeter, all the Mueller matrix elements are simultaneously obtained from 16 frequencies in a Fourier analysis of time-dependent light intensity. The 4-PEM polarimeter can also be operated at oblique angles of incidence so as also to obtain data in reflection like an ellipsometer [12].

This review consists of the following seven sections. Section 2 briefly explains the optical system and characteristic features of the G-HAUP. Sections 3, 4, 5, and 6 describe the recent applications of G-HAUP to salicylidenephenylethylamines [13], alanine [14], benzil [15], and CeF_3 crystals [9]. Finally, Section 7 presents conclusions and future directions for the G-HAUP.

2. Brief description of the G-HAUP method

A schematic representation of the conventional HAUP system is shown in **Figure 1**, which also applies to the G-HAUP. The polarization optics is in both cases composed of two optical elements, a linear polarizer (P) and a linear analyzer (A).

The axes of P and A are set in the crossed Nicols position. The monochromatic light beam emerging from a monochromator or a laser travels through P , the analyte on a sample stage (S), and A successively. Then, the normalized intensity I/I_0 of the light transmitted through P , S , and A is detected with a photomultiplier. θ represents the azimuthal angle of P with respect to a principal axis of the sample, as shown in **Figure 1a**. The positions of P and A are varied systematically from the crossed Nicols position. In addition, Y is defined as the deflection angle of A from perfect extinction. The transmittance can be expressed using the Jones calculus as a function of a matrix for the polarizer, a generalized Jones matrix containing the linear optical effects propagated through a distance, and a Jones matrix for the analyzer [16]. This expression can be reformulated as a quadratic function of the two variables, θ and Y angles.

In the HAUP measurement, because the angle between polarization directions of P and A is set close to 90° , I is weak, such that changes are pronounced and can be well determined by an optical chopper and a lock-in amplifier with a photon-counting system.

The HAUP method requires the accurate evaluation and elimination of systematic errors, notably the parasitic ellipticities p and q originating from P and A , respectively, [3, 4] and a small error angle δY [5]. Here, δY is caused by the slight deviation from the perfect crossed Nicols condition by inserting the sample between P and A .

In summary, the relative intensity ratio Γ of the transmitted light I to the incident light I_0 is obtained by multiplying the Jones vectors of \mathbf{P} and \mathbf{A} and the Jones matrix \mathbf{M}_H and several approximations and coordinate transformations, as follows:

$$\Gamma(\theta', Y', \text{LB, LD, CB, CD}, p, q, \delta Y) = I/I_0 = |\mathbf{A}^T \mathbf{M}_H \mathbf{P}|^2 = A'' + B'' Y' + C'' Y'^2 \quad (1)$$

where

$$A'' = H''_{11} + H''_{12} \theta' + H''_{13} \theta'^2.$$

$$B'' = H''_{21} + H''_{22} \theta'.$$

$$C'' = H''_{31}.$$

Each coefficient of the quadratic function of Γ contains the information of θ' , Y' , LB, LD, CB, CD, and systematic errors p , q , and δY . Therefore, LB, LD, CB, and CD can be recovered by measuring I at various θ' and Y' and eliminating the systematic errors.

Here, we would like to point out the requirements of the samples for G-HAUP measurement. As for other optical measurements, transparent, homogeneous, surface-flat, and defect-free samples are preferred for G-HAUP measurements. In addition, although the details are described elsewhere [9], to avoid anomalous behavior near the unstable and low-sensitivity wavelength regions, samples with a small change in the total phase difference with respect to wavelength are also preferred. To fulfill such requirements, we prepared very thin samples for G-HAUP measurements.

The HAUP has been applied to investigate OA of various crystals such as amino acids [17, 18], proteins [19], chiral co-crystals [20], triglycine sulfate (TGS) [21, 22], as well as KH_2PO_4 (KDP) [23] and $\text{NH}_4\text{H}_2\text{PO}_4$ [24] and their isomorphs.

Furthermore, to measure CD and LD in absorbing crystals of low symmetry, the HAUP method has been extended by various researchers [7, 25, 26]. We have

developed the extended HAUP method for measuring temperature dependencies of LB, LD, CB, and CD simultaneously in a tris(ethylenediamine) cobalt(III) triiodide monohydrate crystal [27]. The recent applications of G-HAUP are wavelength dependencies of chiroptical measurements for laminated collagen membranes with highly preferred orientation [28] and crystals of azobenzene-intercalated $K_4Nb_6O_{17}$ [8], γ -glycine [29], salicylidenephenylethylenamines [13], *L*-alanine [14], benzil [15], and CeF_3 [9]. In the following sections, analyses of the latter four systems by the G-HAUP are summarized.

3. Chiral photomechanical crystals

The chiral single crystals of *S*- and *R*-enantiomers of *N*-3,5-di-*tert*-butylsalicylidene-1-phenylethylamine in the enol form [enol-(*S*)-1 and enol-(*R*)-1] (Figure 2) show photomechanical motion under UV light irradiation [30], that is, light-driven macroscale mechanical motion. Photochromic crystals are often good candidates for photomechanical motion. Upon photoirradiation, the making or breaking of chemical bonds can lead to color changes as well as stresses manifest as macroscale mechanical motion. Photomechanical motion involves the direct conversion of light energy to mechanical energy, and thus, photomechanical crystals may be beneficial for energy conversion. Previous reports show that the dissymmetry of chiral crystals can be manifested in the photomechanical behavior of chiral crystals as opposed to racemic crystals [31, 32].

Enantiomeric salicylidenephenylethylenamines enol-(*S*)-1 and enol-(*R*)-1 (Figure 2) before and under UV light irradiation were analyzed by the G-HAUP method in order

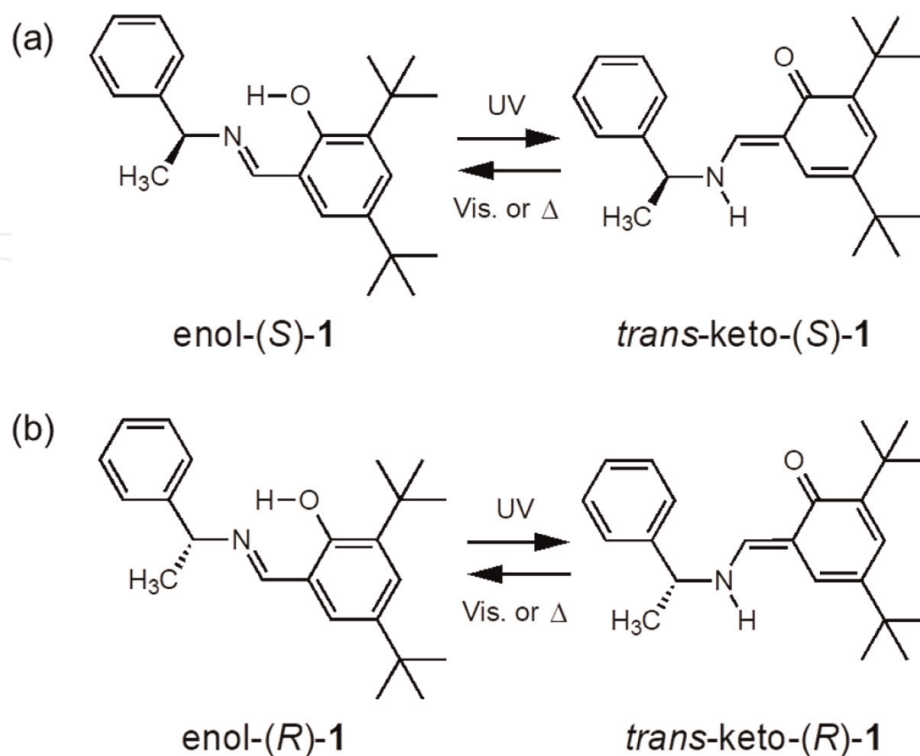


Figure 2. Photoinduced hydrogen transfer reaction of salicylidenephenylethylenamines enol-(*S*)-1 (a) and enol-(*R*)-1 (b). Reproduced from ref. [13] with permission from the American Chemical Society.

to obtain LB, LD, CB, and CD spectra and subsequently to correlate the changes of the optical properties to the changes of the crystal structures during the photoreaction [13].

Compounds enol-(*S*)-**1** and enol-(*R*)-**1** were synthesized according to a published protocol, and the single crystals of enol-(*S*)-**1** and enol-(*R*)-**1** were grown by sublimation at 10–20°C below the melting points (92–93°C).

At the outset, the crystal structure of enol-(*S*)-**1** had already been determined, but not that of *trans*-keto-(*S*)-**1** [30]. Hence, *in situ* crystallographic analyses were carefully performed under continuous UV irradiation to analyze the crystal structure of *trans* photoproduct. Because no disorder was found in the crystals, we calculated the crystal structure of *trans*-keto-(*S*)-**1** by dispersion-corrected density functional theory (DFT) calculations (Figure 3b). As shown in Table 1, the *a* and *b* axes contracted, and the *c* axis extended.

Figure 4 shows the LB, LD, CB, and CD spectra of the enol-(*S*)-**1** (thickness: 6.5 μm) and enol-(*R*)-**1** (thickness: 7.6 μm) crystals through the (001) face before UV irradiation. The LB and LD spectra between the *S* and *R* enantiomeric crystals are coincident (Figure 4a and b), because linear anisotropies are not affected by enantiomorphism. The negative LD peak at 330 nm corresponds to the π - π^* transition of the intramolecularly hydrogen-bonded salicylideneimino moiety. The LB spectra exhibited anomalous dispersion of negative peaks at 360 nm with a change in sign at the strong LD peak. These results show that the LB and LD spectra satisfy the

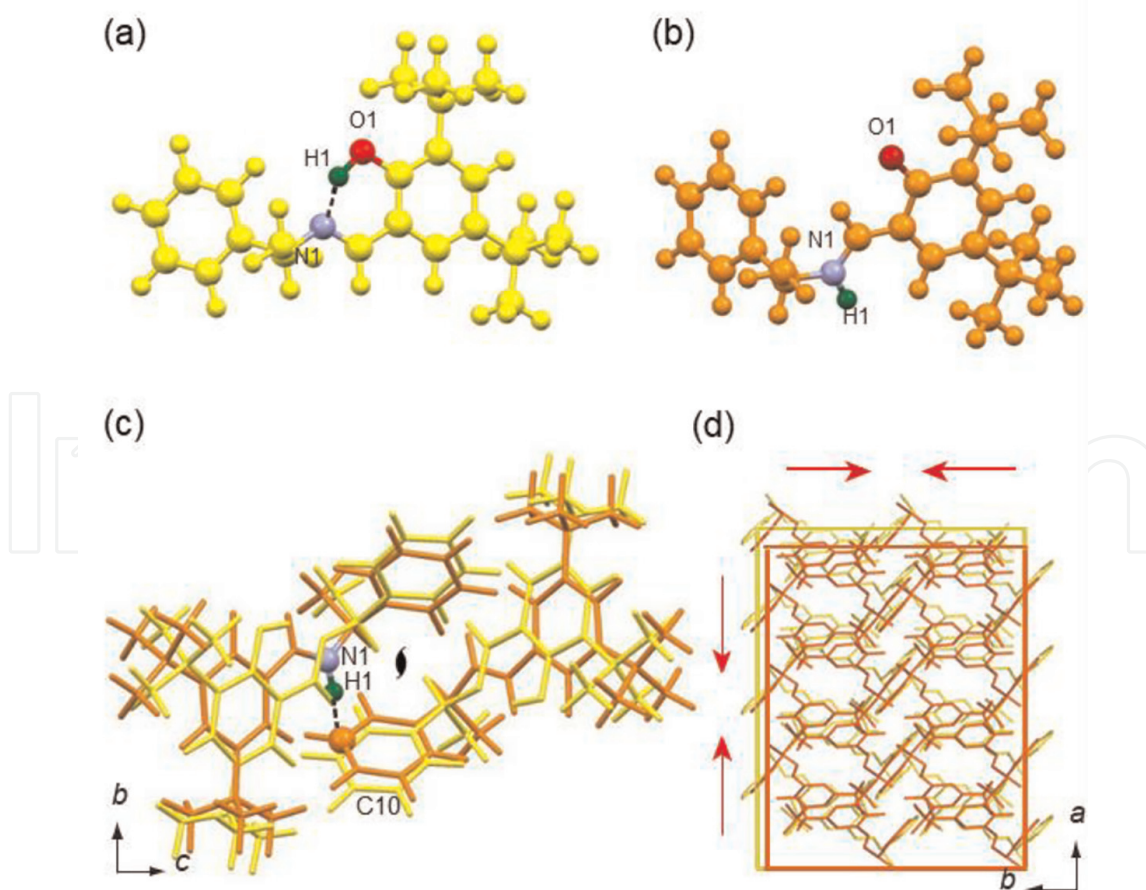


Figure 3. Calculated crystal structures: Ball-and-stick drawings of (a) enol-(*S*)-**1** (yellow) and (b) *trans*-keto-(*S*)-**1** (orange). Tautomer structures overlaid on the (c) (100) and (d) (001) faces. The red arrows in (d) show the direction of contraction of the *trans*-keto-(*S*)-**1** crystal along *a* and *b* axes. Reproduced from ref. [13] with permission from the American Chemical Society.

	enol-(S)-1	trans-keto-(S)-1	Relative change (%)
a (Å)	6.080	5.856	-3.70
b (Å)	9.633	9.313	-3.32
c (Å)	35.454	35.509	+0.16
V (Å ³)	2076.630	1936.486	-6.75

Table 1. Unit cell dimensions of enol-(S)-1 by X-ray diffraction and trans-keto-(S)-1 crystals obtained from DFT calculations. Reproduced from ref. [13] with permission from the American Chemical Society.

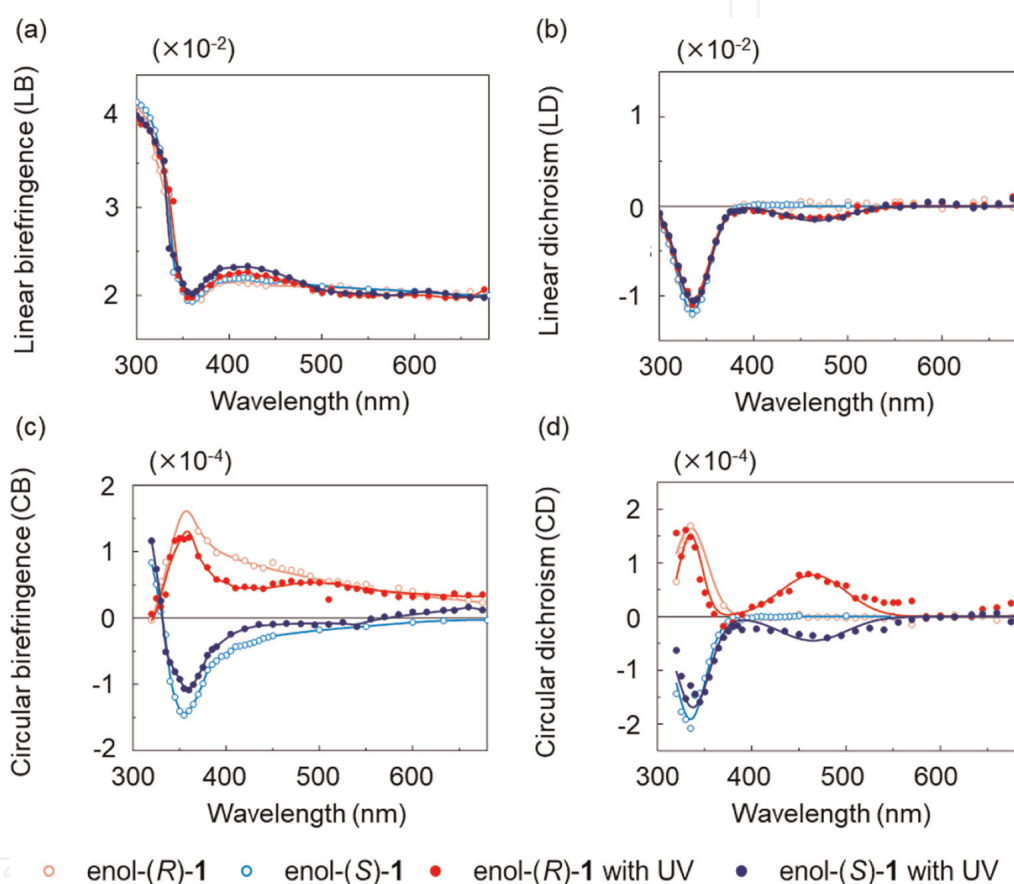


Figure 4. Optical anisotropic and chiroptical spectra of enol-(S)-1 and enol-(R)-1 crystals on the (001) face: (a) LB, (b) LD, (c) CB, and (d) CD. These properties were measured with the G-HAUP in the dark and under continuous UV light irradiation at 365 nm. The curved lines are fitted gaussian functions intended to guide the eye (a, c). Reproduced from ref. [13] with permission from the American Chemical Society.

Kramers–Kronig relationship [33]. The CD spectra of enol-(S)-1 and enol-(R)-1 crystals revealed, respectively, a strong negative and positive Cotton effect at 330 nm, which mirror each other (**Figure 4d**). The CB spectra of enol-(S)-1 and enol-(R)-1 crystals also exhibited anomalous dispersion of negative and positive peaks at 360 nm with changes in sign at the CD peaks (**Figure 4c**), respectively, indicating that the Kramers–Kronig relationship also holds between CB and CD.

We then attempted to measure the LB, LD, CB, and CD spectra of both enantiomeric enol-1 crystals under UV irradiation with a 365 nm LED directed normal to the G-HAUP light path at low power (5 mW cm^{-2}) to minimize incident UV light reaching the detector. UV irradiation-induced bending was inhibited by fixing the crystals to a

plate with silicone grease. Note that salicylidenephenylethylamines, which were used in this study, do not show thermochromism. **Figure 4** also shows the LB, LD, CB, and CD spectra under continuous UV irradiation at 365 nm, which represents the spectra at the photostationary state of the reactant and product. New LD peaks corresponding to *trans*-keto-(*S*)-**1** and *trans*-keto-(*R*)-**1** appeared at around 460 nm, and the magnitudes of the LD peaks at 330 nm decreased slightly. The LD spectra of the *S* and *R* *trans*-keto isomers were coincident (**Figure 4b**). New, small negative and positive CD peaks appeared at 460 nm due to the formation of *trans*-keto-(*S*)-**1** and *trans*-keto-(*R*)-**1** crystals, respectively, and the magnitudes of CD peaks at 330 nm decreased slightly (**Figure 4d**). The CB spectra also exhibited anomalous dispersions of negative [enol-(*S*)-**1**] and positive [enol-(*R*)-**1**] peaks at 500 and 360 nm with a change in sign at the new CD peak (**Figure 4c**), as with the LB and LD spectra. The Kramers–Kronig transformation related the CB to the CD and the LB to the LD.

The LB of both enantiomeric enol-**1** crystals along the *c*-axis showed a relatively lower value (0.02) above 600 nm than the previously reported organic crystals [8, 17–20, 28, 34, 35]. The total intermolecular interaction in the enol-(*S*)-**1** crystal along all directions is the van der Waals force alone. This very weak molecular interaction may have induced such a small LB. In fact, we have reported a much larger value (0.4) for the LB of the chiral cocrystal composed of tryptamine and 4-chlorobenzoic acid [20]. This cocrystal exhibits strong intermolecular interactions, such as ionic bridging and the hydrogen bonding. The optical rotatory power (ORP) value of enol-(*S*)-**1** crystals along the *c*-axis at 632.8 nm before UV irradiation was calculated to be -5.2 deg./mm. The signs of ORP dispersion along the *c*-axis are opposite to those in the hexane solution, the orientationally averaged value [13]. This suggests that the contribution from the ORP dispersion along the *c*-axis might be small, or the ORP dispersions along the *a*- and/or *b*-axes might be largely positive in sign. The dissymmetry parameter, *g*, in the crystalline state is defined as the ratio in absolute magnitude of CD to absorbance. The *g* value of enol-(*S*)-**1** crystal along the *c*-axis was calculated to be 0.013. On the other hand, the *g* value of enol-(*S*)-**1** in hexane solution was calculated to be 0.0010, revealing that the *g* value of the enol-(*S*)-**1** crystal obtained by the G-HAUP measurement without UV irradiation is around 10 times larger than *g* values in the solution and by the calculation in Ref [13].

4. Chiral alanine crystal

L-alanine is the smallest chiral natural amino acid. As an additive in ferroelectric triglycine sulfate crystals, it can control the crystal polarity, which is of practical use in infrared detectors. *L*-alanine alone grows as large, hard, transparent crystals [36] from evaporating solutions in the space group $P2_12_12_1$ [37, 38]. Thus, alanine is an optically biaxial chiral crystal with four zwitterionic molecules ($^+H_3NCH(CH_3)COO^-$) in the unit cell. Misoguti *et al.* [39] measured the dispersion of refractive indices, among the many other physicochemical properties that have been investigated [40–43], but the anisotropy of the optical activity has not been established.

We measured the wavelength dependence of the CB of alanine crystals along each crystallographic axis, by G-HAUP, and assigned the absolute structure of the crystals examined by the method of anomalous dispersion to determine the absolute chirality of alanine crystals, by correlating the absolute structure obtained with the X-ray diffraction method with the CB measured using the G-HAUP.

L- and *D*-alanine crystals were grown by solvent evaporation using the enantiomeric *L*- and *D*-alanine powder as solute and DIW as solvent. Samples for crystal structure determination and the measurement of CB (and optical activity, OA = CB/2) were prepared from these crystals.

The results from the X-ray crystal structure analyses are shown in **Table 2**. The unit cell parameters are almost the same as those from the previous study. Furthermore, we succeeded in determining the absolute structure of the *L*- and *D*-alanine crystals.

For the measurements of chiroptical properties, crystals were cut perpendicular to the <010> direction and (010) faces of *L*- and *D*-alanine crystals were polished to 21 μm and 13 μm, respectively, by using lapping films with SiC (5.0 μm), Al₂O₃ (1.0 μm), and FeO (0.3 μm) abrasive, successively. The polished crystals were fixed on a pinhole and chiroptical properties were measured. The values of LB, LD, and OA in the <010> direction were obtained (**Figure 5**). LB clearly decreases and approaches zero with decreasing wavelength (**Figure 5a**), while LD is almost zero from 280 to 680 nm (**Figure 5b**). LB in the <010> direction is significantly smaller than that in the <100> direction, which allows G-HAUP to detect OA more sensitively. The magnitude of OA is almost the same in *L*- and *D*-alanine crystals, but their signs are opposite as shown in **Figure 5c**. Consequently, *L*- and *D*-alanine crystals exhibit positive and negative OA in the <010> direction, respectively, which means *L*- and *D*-alanine crystals are *levorotatory* and *dextrorotatory*, respectively, in this direction, over the spectrum evaluated.

The interpretation of the results of HAUP studies remains a challenge. In a study of the CB of crystals of *L*-glutamic acid, we introduced the *chirality index*, $r = 1 - |\rho_s|/|\rho_c|$, where $|\rho_s|$ is the absolute optical rotation per molecule in solution and $|\rho_c|$ is the optical rotation per molecule in the crystal averaged over the eigenvalues of the gyration tensor. Values close to 1 are dominated by the effects of crystallization. For *L*-alanine, $r = 0.999$, indicating that the OA is principally a crystal-optical effect.

No general, quantum chemical methods [44] have yet been implemented in widely distributed electronic structure computing programs for interpreting the chiroptical effects of molecular crystals. However, progress is on the horizon. Linear response theories with periodic boundary conditions are required because the OA of molecules is strongly affected by the environment, as confirmed by experimental and computational

	<i>L</i> -alanine	<i>D</i> -alanine	Simpson Jr. and Marsh [37]
Temperature (K)	173	173	298
Crystal system	Orthorhombic	Orthorhombic	Orthorhombic
Space group	<i>P</i> 2 ₁ 2 ₁ 2 ₁	<i>P</i> 2 ₁ 2 ₁ 2 ₁	<i>P</i> 2 ₁ 2 ₁ 2 ₁
<i>a</i> (Å)	5.9753(1)	5.9701(4)	6.032(1)
<i>b</i> (Å)	12.2966(2)	12.2935(7)	12.343(1)
<i>c</i> (Å)	5.7895(1)	5.7933(6)	5.784(1)
<i>Z</i>	4	4	4
<i>R</i> ₁	0.0250	0.0297	0.049
<i>wR</i> ₂	0.0730	0.0764	—
Flack parameter	−0.16(9)	−0.01(11)	—

Crystal data for L- and D-alanine crystals. Reproduced from ref. [14] with permission from Elsevier.

Table 2.
 Crystal data for *L*- and *D*-alanine crystals.

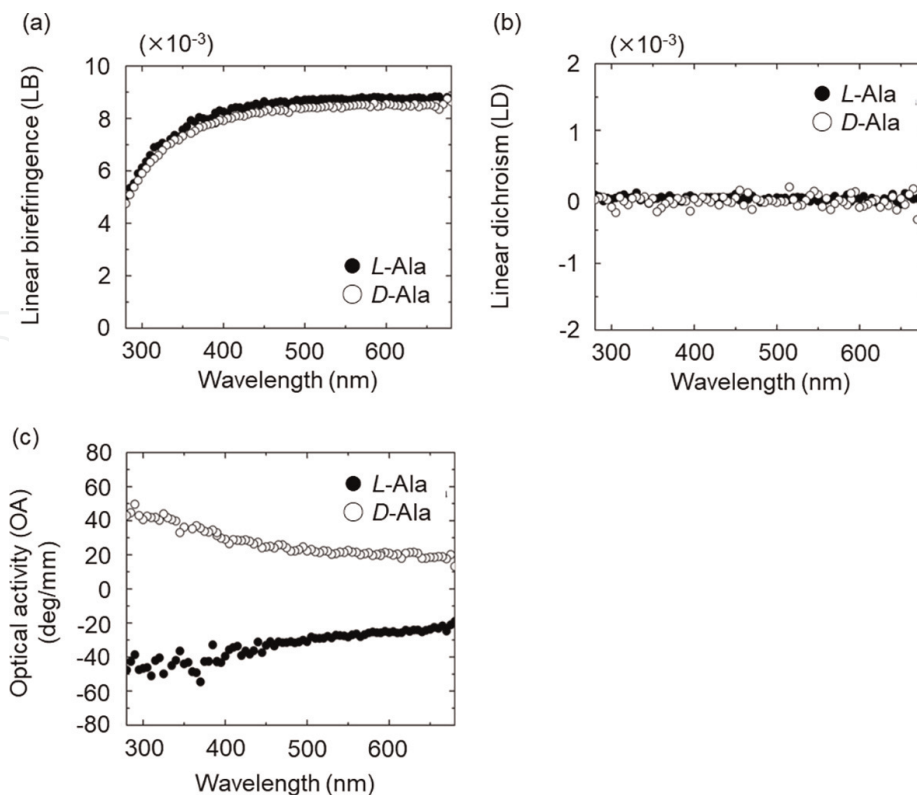


Figure 5. Wavelength dependence of LB (a), LD (b), and OA (c) in the $\langle 010 \rangle$ direction of L- and D-alanine crystals. Closed and opened circles are results for L- and D-alanine, respectively. Reproduced from ref. [14] with permission from Elsevier.

studies on the solvent dependence of OR [45], in addition to many studies of computational investigations of crystallographic supercells that we performed over the years. To minimize the effects of interfacial molecules, larger and larger aggregates of molecules must be computed, a process that becomes intractable, as illustrated in the following section for benzil. Balduf and Caricato made this convergence problem explicit *in silico* for F_2 and HF molecules arranged as model helices [46]. Unit cells were inadequate representations of large helices. More recently, Rérat and Kirtman have introduced computed results of the chiroptical properties of periodic systems using the self-consistent coupled-perturbed method in the program suite CRYSTALS [47].

The relationship between the absolute structure and OA along the b -axis was considered parallel to the twofold screw axes considered for L-alanine. The hydrogen bond chains for L- and D-alanine were, respectively, right and left handed (**Figure 6**). However, there is no simple prescription for correlating configuration with the sense of optical rotation. This is true for crystals as for molecules.

From a classical perspective, a right-handed helix of atoms/molecules might be dextrorotatory or levorotatory depending on the polarizability of the groups decorating the helix. From a quantum mechanical perspective, identifying the relevant chromophores is requisite. Furthermore, individual bands may contribute to the CB positively or negatively.

5. Chiral benzil crystal

Benzil ($C_6H_5C(O)-C(O)C_6H_5$) crystals have been considered the organic analogue of quartz; both substances have D_3 point symmetry and can be obtained

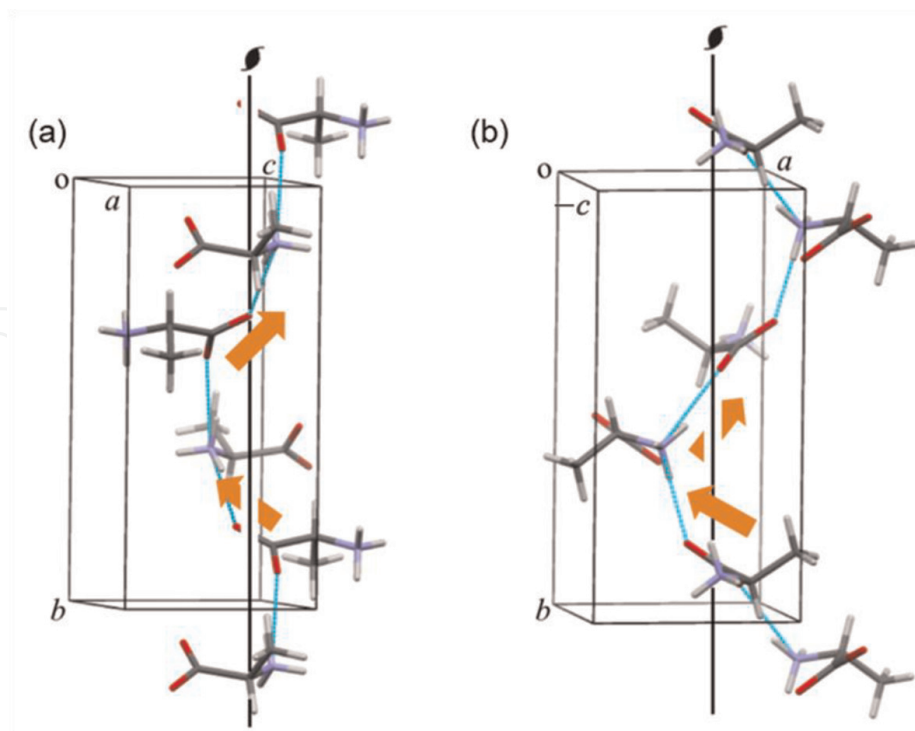


Figure 6.
The handedness of the twofold screw axis of alanine crystals along the b-axis. (a) L-alanine and (b) D-alanine. Reproduced from ref. [14] with permission from Elsevier.

as large single crystals. The OA of benzil has been studied more than that of any other organic crystal; however, unlike quartz, its OA anisotropy has resisted characterization. Without measurements of the optical activity along the diad axes, as opposed to the easily measured optic axis where $LB = 0$, interpretations are incomplete. Here, we compare OA measurements along the low-symmetry direction of crystalline benzil by the G-HAUP accompanied by electronic structure calculations of the benzil molecule and aggregates of benzil molecules based on the crystal structure.

Single crystals of benzil were grown by slow evaporation from acetone at 25°C. Plates (5 mm × 5 mm × 1 mm) were cut with a razor blade, exposing large (001) or (100) faces. Samples were then polished sequentially with SiC (grain diameter 9 and 5 μm), Al₂O₃ (3 and 1 μm), and Fe₂O₃ (0.3 μm) lapping films. Single-crystal X-ray diffraction analysis confirmed the enantiomorphous space groups $P3_1(2)21$ (Figure 7). While the structure of benzil has been established previously [48], the absolute structure was determined first in the aforementioned citation.

A *c*-cut slab of $P3_121$ benzil measuring 26.2 μm was analyzed. The OA along the optic axis was easily measured by rotating the analyzer to the extinction position in the G-HAUP. For the $P3_121$ enantiomorph, benzil is *dextrorotatory* at optical frequencies (Figure 8c). The OA along the *c*-axis is 24.3°/mm at 590 nm, in good agreement with sodium D-line (25°/mm) measurements [49, 50].

An 88 μm thick *a*-slab of $P3_121$ benzil was likewise polished. The LB, LD, OA, and CD were successfully extracted, and the dispersion in Figure 8 was fit to a simple Drude oscillator:

$$\rho = \frac{A}{\lambda^2 - \lambda_i^2}, \quad (2)$$

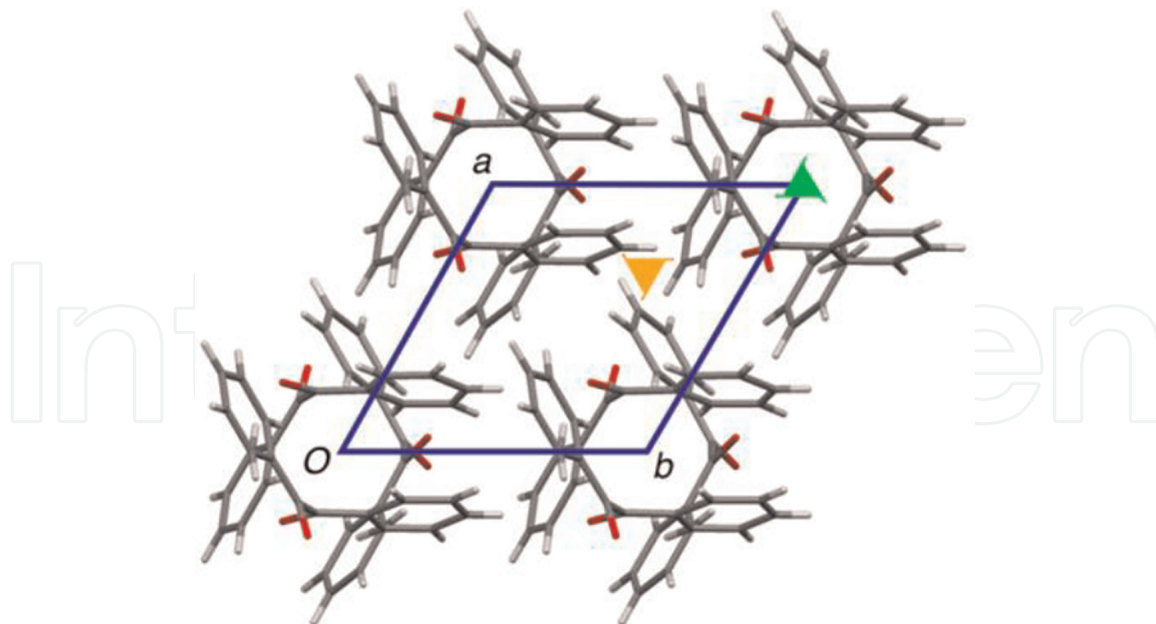


Figure 7. Unit cell of $P3_121$ crystalline benzil viewed along $[001]$ with the 3_1 axes in green and orange. Reproduced from ref. [15] with permission from the American Chemical Society.

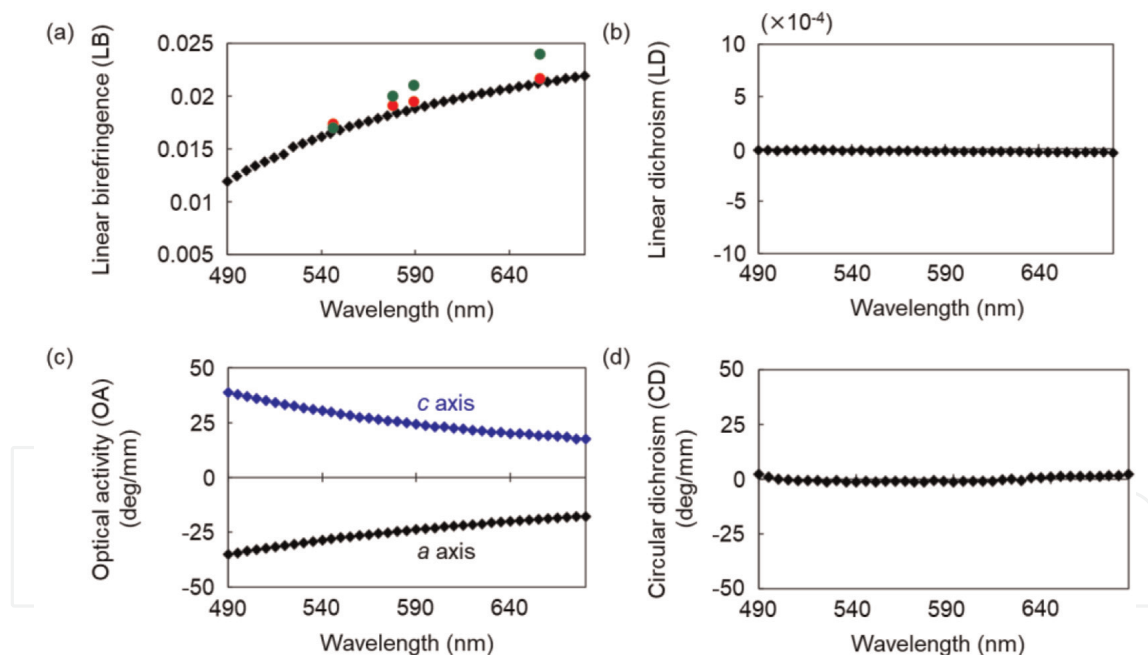


Figure 8. Wavelength dependences of LB (a), LD (b), fitted OA (c), and CD (d) of the $P3_121$ benzil crystal. (a) Published values at fixed wavelengths are red [51] and green [52] points. (c) The OA was fitted to an oscillator model (see text). For the $P3_121$ enantiomorph, the OA along the c- and a-axes at 590 nm is 24.3 deg./mm and -23.8 deg./mm, respectively. Reproduced from ref. [15] with permission from the American Chemical Society.

where A and λ_l are constants with fitted values of 7.9462×10^6 and 117.18 nm, respectively. The LB perpendicular to the optic axis and OA along the optic axis agreed well with literature values [49–52].

The long wavelength (589 nm) OA tensors of one benzil molecule, three benzil molecules in the unit cell, and three benzil molecules related by a threefold rotation

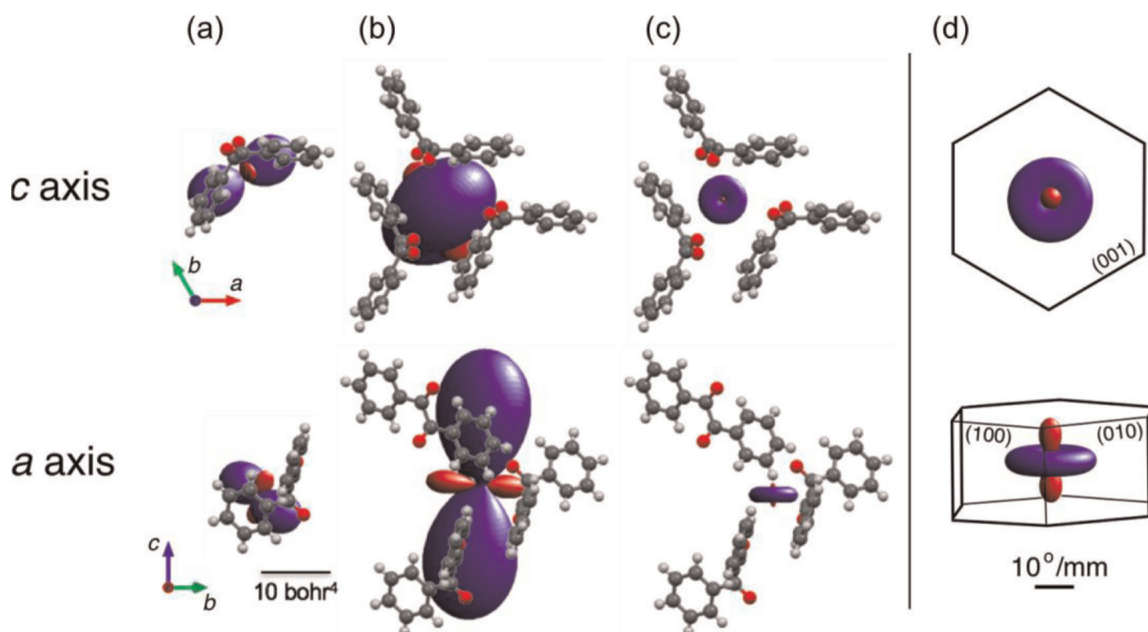


Figure 9. Representation surfaces of the computed long wavelength OA of benzil at 589 nm (plotted with the software WinTensor, W. Kaminsky). (a) One molecule in the gas phase, (b) one unit cell treated of three molecules, (c) one unit cell based on results for one molecule in (a) and symmetrized, and (d) experimental result based on G-HAUP data. Reproduced from ref. [15] with permission from the American Chemical Society.

(as opposed to a threefold screw) were calculated using well-known methods [53, 54]. The results are summarized in **Figure 9**. The calculations of a small number of molecules are a poor mimic of the crystallographic response.

Benzil and 4-methylbenzophenone [55] are the only such examples of molecular crystals dominated by weak intermolecular interactions for which the long-wavelength OA anisotropy has been determined. Unfortunately, because benzil is in dynamic equilibrium in solution, it is not amenable to a calculation of the chirality index, r (see above).

Interpreting this tensor in terms of a small number of excited states is difficult because unlike simple hydrocarbons investigated previously [56, 57], a great number of states contribute to the long-wavelength value of benzil. Requisite for the computation of chiroptical properties in crystals is the development of linear response theory with periodic boundary conditions to provide a framework for interpreting the results of single-crystal polarimetry, as discussed above.

6. Magneto-optical CeF₃ crystal

Frequency instabilities and parasitic oscillations in optical sources are deleterious to a civilization increasingly dependent on the transfer of optical information with light. An optical isolator is an optical diode that allows light to pass in only one direction. The functions of optical isolators are based on the non-reciprocal magneto-optical rotation of polarization of light, long known as the Faraday rotation (FR). The crystals investigated and employed as optical isolators to date include only isotropic crystals or uniaxial crystals with well-defined isotropic directions (*i.e.*, along the optic axis). Otherwise, optically anisotropic crystals are complicated by LB and LD.

Like OA, FR in anisotropic crystals cannot be accurately measured conventionally, except along high-symmetry directions. Therefore, low-symmetry directions in anisotropic crystals have been avoided in magneto-optical research.

A sample subjected to a magnetic field applied parallel and anti-parallel to the wave vector of the light can manifest FR and magnetic circular dichroism (MCD) that can be analyzed by the G-HAUP method. A Nd-Fe-B (NIB) magnet introduced for this purpose is shown in **Figure 10**. In this configuration, we measured the dispersion of FR and MCD in CeF_3 single crystal along the optic axis (c -axis) as well as *perpendicular* to the optic axis (a -axis) with the G-HAUP.

Single crystals of CeF_3 were grown by the modified Czochralski technique [58–60]. We prepared two types of samples: (001) and (100) plates of single-crystal CeF_3 . The smooth flat sample surfaces were obtained by polishing machines with a diamond slurry (3.0 μm) and colloidal silica (32.5 nm) abrasive, successively. We polished a 307 μm thick (001) plate of a single crystal of CeF_3 [58–60] with point symmetry D_{3d} . When the magnetic field was applied parallel to the light propagation direction, FR occurs only along $\langle 001 \rangle$. In this direction, the measurement is conventional, but here, we implemented the rotating analyzer mode of G-HAUP. The sample was sandwiched between two permanent NIB magnets and illuminated through a 0.5 mm pinhole (**Figure 10**). The longitudinal field of ~ 0.5 Tesla (T) was homogeneous [60]. The wavelength dependence of the Verdet constant, the quantity in $\text{deg./mm}\cdot\text{T}$ that describes the strength of FR along the c -axis at 25°C , is plotted as black rhombuses in **Figure 11c**. Positive Verdet constants along the c -axis indicated that the right-handed

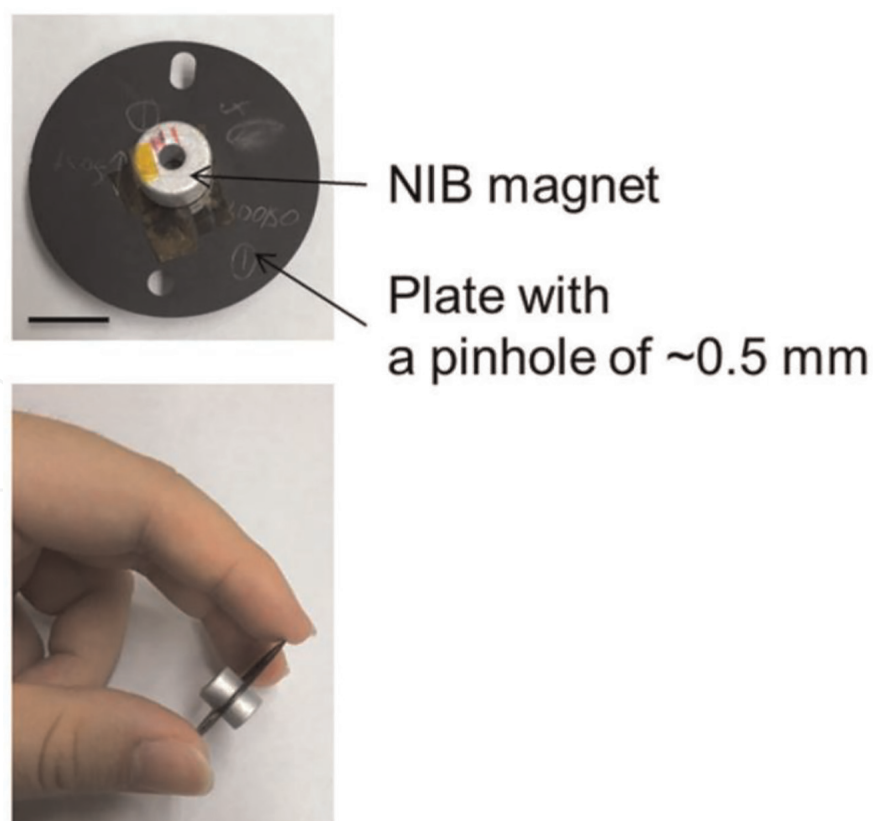


Figure 10.

Photograph of the Nd-Fe-B (NIB) magnet with the magnetic field applied parallel or anti-parallel to the light propagation direction. The sample was mounted on a plate with a ~ 0.5 mm pinhole sandwiched between two identical NIB permanent magnet rings. The black scale bar = 1 cm. Reproduced from ref. [9] with permission from Springer Nature.

circularly polarized light propagates faster than its left-handed counterpart across the spectrum.

A (100) plate just 58.0 μm thick was polished. The extinction directions were determined accurately with an Ehringhaus compensator fitted to a polarized light microscope. We first determined with G-HAUP in the extended mode the dispersion of LD, OA, and CD along the a -axis in the absence of the magnetic field at 25°C (blue rhombuses in **Figure 11**). LB was comparable to that of α -quartz (**Figure 11a**). LD was almost zero over the wavelength examined (**Figure 11b**), consistent with the absence of absorption bands at wavelengths longer than 282 nm. The OA and CD values were also close to zero, consistent with the D_{3d} symmetric crystal structure. The dispersion of LB, LD, FR, and MCD along $\langle 100 \rangle$ was established, while the magnetic field was propagated parallel and anti-parallel to the wave vector at 25°C (red rhombuses in **Figure 11**). LB and LD were indifferent to the sign of the magnetic field. Reversing the magnetic field direction inverted the signs of FR and MCD. The values of LB and LD hardly changed with and without the magnetic field (**Figure 11a** and **b**). The Verdet constants along the a -axis were positive throughout the wavelength region (**Figure 11c**).

CeF_3 is paramagnetic at room temperature. Therefore, the magnetic interactions such as ferromagnetism, anti-ferromagnetism, or ferrimagnetism, which are often observed in low-temperature regions, do not affect the G-HAUP measurements. Cerium is usually in the 3+ oxidation state in condensed matter; the electronic

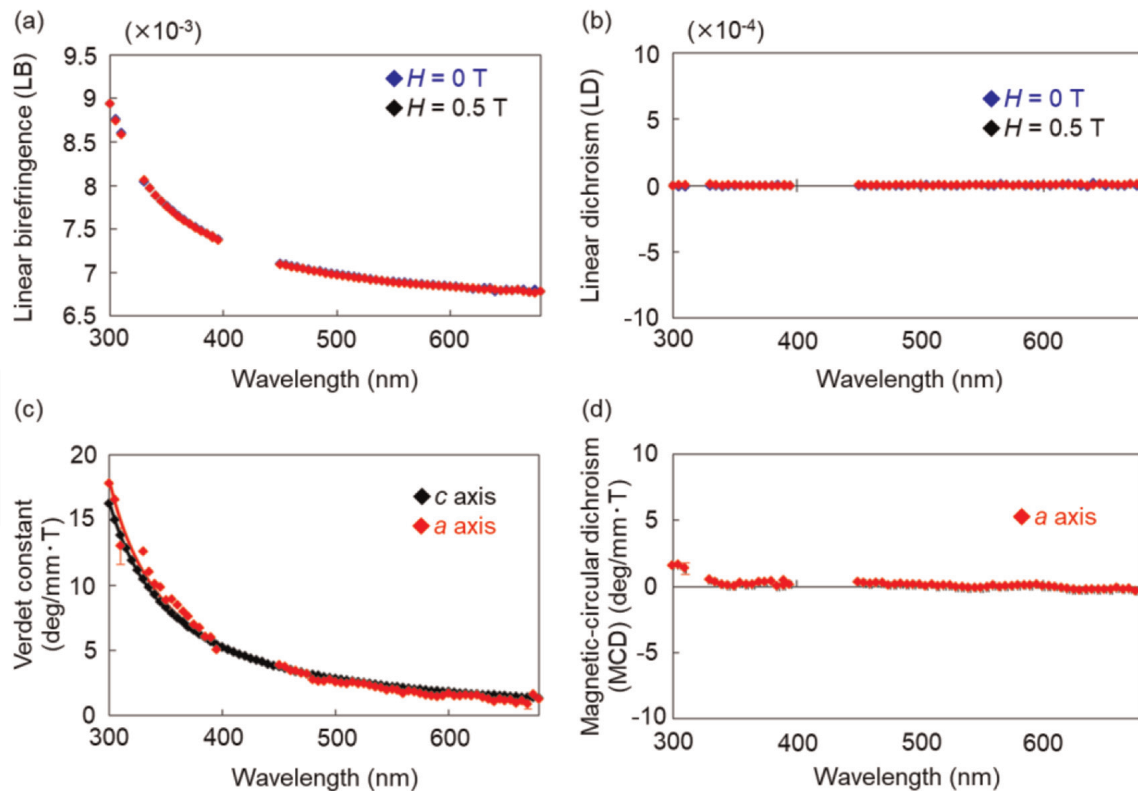


Figure 11. Wavelength dependences of LB (a), LD (b), Verdet constant (c), and MCD (d) in single-crystal CeF_3 at 25°C. the black, blue, and red rhombuses represent the data along $\langle 001 \rangle$, along $\langle 100 \rangle$ without a magnetic field, and along $\langle 100 \rangle$ under an applied magnetic field, respectively. We eliminated points in spectral regions where G-HAUP is less sensitive. The Verdet constant spectra were fitted to a simple Drude oscillator. The error bars represent the standard deviations. The error along $\langle 100 \rangle$ given in (c) ranged from 0.32 to 1.40 $\text{deg}/\text{mm}\cdot\text{T}$. reproduced from ref. [9] with permission from Springer Nature.

configuration of Ce^{3+} is $1s^2 2s^2 2p^6 \dots 4d^{10} 4f^1 5s^2 5p^6$. Transitions from $4f \rightarrow 5d$ confer the magneto-optical properties in the UV-Vis-IR region [61]. The Verdet constants were positive along the c - and a -axes at all measured wavelengths, and their magnitudes along both axes were nearly equal (**Figure 11c**). The magnetic susceptibilities, measured with SQUID (superconducting quantum interference device), were nearly identical in both directions. The magnitude of Verdet constants at an arbitrary frequency depends on the magnetic susceptibility and the transition probabilities. Therefore, we may surmise that the anisotropy of the summed $4f \rightarrow 5d$ transition probabilities is zero.

7. Conclusions

In this review, principles and recent applications of G-HAUP method are concisely introduced. New CD peaks in photomechanical crystals originating from photochromism were observed. According to the G-HAUP results of alanine crystals, we discuss the relationship between the absolute structure and OA. In addition, we found by benzil measurements and quantum chemical calculations that the intermolecular interactions are decisive even though comparatively weak dispersion forces dominate the interactions between molecules. Moreover, the first application of G-HAUP to a magneto-optical material was presented by applying magnetic field with NIB magnets. These results strongly indicate the usefulness of the HAUP method for evaluating the chiroptical and magneto-optical properties of ordered specimens. More recently, a rapid HAUP system was developed by using dispersive detection technique with a CCD array spectrometer [62]. Very thin crystalline sample, *ca.* less than several dozen micrometers, were prepared to accommodate the G-HAUP transmission requirement. A reflection-mode HAUP system can contribute to the significant increase in the number of HAUP-applicable specimen because of the simplification of sample preparation. In addition, the extension of wavelength coverage to the infrared and/or vacuum UV region results in the significant increase in the information related to the electronic structure and/or conformation of optically active specimens [63].

Acknowledgements

This review is cordially dedicated to Prof. Jinzo Kobayashi, who is an inventor of HAUP and has opened a new way to solid-state dissymmetry from a spectroscopic point of view. We thank Prof. Dr. Hidehiro Uekusa, Prof. Dr. Tadashi Mori, Dr. Alexander T. Martin, Dr. Shane M. Nichols, and Dr. Veronica L. Murphy for their fruitful discussions and comments. This study was financially supported by the JSPS Scientific Research in the Challenging Exploratory Research, the High-Tech Research Center (TWIns), the Consolidated Research Institute for Advanced Science and Medical Care (ASMeW), the Global COE for Practical Chemical Wisdom, the Leading Graduate Program in Science and Engineering, the Top Global University Project, Waseda University, from the Ministry of Education, Culture, Sports, Science and Technology, Japan, and the grant-in-aid from the Mitsubishi Materials Corporation and the Mizuho Foundation for the Promotion of Sciences.

Conflict of interest

The authors declare no conflict of interest.

IntechOpen

Author details

Toru Asahi^{1,2*}, Masahito Tanaka³, Kenta Nakagawa^{1,4*}, Yukana Terasawa^{1,4}, Kazuhiko Ishikawa¹, Akifumi Takanabe¹, Hideko Koshima² and Bart Kahr⁵

1 Graduate School of Advanced Science and Engineering, Waseda University, Tokyo, Japan

2 Research Organization for Nano and Life Innovation, Waseda University, Tokyo, Japan


3 National Institute of Advanced Industrial Science and Technology (AIST), Tokyo, Japan

4 Kagami Memorial Research Institute for Materials Science and Technology, Waseda University, Tokyo, Japan

5 Department of Chemistry and Molecular Design Institute, New York University, New York, USA

*Address all correspondence to: tasahi@waseda.jp and kenta.nakagawa@aoni.waseda.jp

IntechOpen

© 2022 The Author(s). Licensee IntechOpen. This chapter is distributed under the terms of the Creative Commons Attribution License (<http://creativecommons.org/licenses/by/3.0>), which permits unrestricted use, distribution, and reproduction in any medium, provided the original work is properly cited. 

References

- [1] Claborn K, Isborn C, Kaminsky W, Kahr B. Optical rotation of achiral compounds. *Angewandte Chemie (International Ed. in English)*. 2008;**47**: 5706-5717. DOI: 10.1126/science.1173605
- [2] Kahr B, Arteaga O. Arago's best paper. *ChemPhysChem*. 2012;**13**:79-88. DOI: 10.1002/cphc.201100660
- [3] Kobayashi J, Asahi T, Takahashi S, Glazer AM. Evaluation of the systematic errors of polarimetric measurements: Application to measurements of the gyration tensors of α -quartz by the HAUP. *Journal of Applied Crystallography*. 1988;**21**:479-484
- [4] Kobayashi J, Uesu Y. A new optical method and apparatus 'HAUP' for measuring simultaneously optical activity and birefringence of crystals. I. Principles and construction. *Journal of Applied Crystal*. 1983;**16**:204-211. DOI: 10.1107/S0021889883010262
- [5] Kobayashi J, Kumomi H, Saito K. Improvement of the accuracy of HAUP, high-accuracy universal polarimeter: Application to ferroelectric $[\text{N}(\text{CH}_3)_4]\text{ZnCl}_4$. *Journal of Applied Crystallography*. 1986;**19**:377-381. DOI: 10.1107/S0021889886089197
- [6] Asahi T, Kobayashi J. Polarimeter for anisotropic optically active materials. In: Weiglhofer WS, Lakhtakia A, editors. *Introduction to Complex Mediums for Optics and Electromagnetics*. Washington: SPIE; 2003. pp. 645-676. DOI: 10.1117/3.504610.ch26
- [7] Kobayashi J, Asahi T, Sakurai M, Takahashi M, Okubo K, Enomoto Y. Optical properties of superconducting $\text{Bi}_2\text{Sr}_2\text{CaCu}_2\text{O}_8$. *Physical Review B*. 1996; **53**:11784-11795. DOI: 10.1103/PhysRevB.53.11784
- [8] Tanaka M, Nakamura N, Koshima H, Asahi T. An application of the advanced high-accuracy universal polarimeter to the chiroptical measurement of an intercalated compound $\text{K}_4\text{Nb}_6\text{O}_{17}$ with high anisotropy. *Journal of Physics D: Applied Physics*. 2012;**45**:175303. DOI: 10.1088/0022-3727/45/17/175303
- [9] Nakagawa K, Asahi T. Determination of the faraday rotation perpendicular to the optical axis in uniaxial CeF_3 crystal by using the generalized-high accuracy universal polarimeter. *Scientific Reports*. 2019;**9**:18453. DOI: 10.1038/s41598-019-54174-2
- [10] Kuroda R, Harada T, Shindo Y. A solid-state dedicated circular dichroism spectrophotometer: Development and application. *The Review of Scientific Instruments*. 2001;**72**:3802-3810. DOI: 10.1063/1.1400157
- [11] Arteaga O, Freudenthal J, Wang B, Kahr B. Mueller matrix polarimetry with four photoelastic modulators: Theory and calibration. *Applied Optics*. 2012; **51**:6805-6817. DOI: 10.1364/AO.51.006805
- [12] Arteaga O, Freudenthal J, Kahr B. Reckoning electromagnetic principles with polarimetric measurements of anisotropic optically active crystals. *Journal of Applied Crystallography*. 2012;**45**:279-291. DOI: 10.1107/S0021889812006085
- [13] Takanabe A, Tanaka M, Johmoto K, Uekusa H, Mori T, Koshima H, et al. Optical activity and optical anisotropy in photomechanical crystals of chiral salicylidenephenylethylamines. *Journal of the American Chemical Society*. 2016; **138**:15066-15077. DOI: 10.1021/jacs.6b09633

- [14] Ishikawa K, Terasawa Y, Tanaka M, Asahi T. Accurate measurement of the optical activity of alanine crystals and the determination of their absolute chirality. *Journal of Physics and Chemistry of Solids*. 2017;**104**:257-266. DOI: 10.1016/j.jpccs.2017.01.024
- [15] Nakagawa K, Martin AT, Nichols SM, Murphy VL, Kahr B, Asahi T. Optical activity anisotropy of benzil. *Journal of Physical Chemistry C*. 2017;**121**:25494-25502. DOI: 10.1021/acs.jpcc.7b08831
- [16] Jones RC. A new calculus for the treatment of optical systems. VII. Properties of the N-matrices. *Journal of the Optical Society of America*. 1948;**38**: 671-685. DOI: 10.1364/JOSA.38.000671
- [17] Asahi T, Utsumi H, Itagaki Y, Kagomiya I, Kobayashi J. Optical activity of crystalline glutamic acids. *Acta Crystallography*. 1996;**A52**:766-769. DOI: 10.1107/S010876739609993X
- [18] Asahi T, Takahashi M, Kobayashi J. The optical activity of crystalline *L*-aspartic acid. *Acta Crystallography*. 1997;**A53**:763-771. DOI: 10.1107/S0108767397004595
- [19] Kobayashi J, Asahi T, Sakurai M, Kagomiya I, Asai H, Asami H. The optical activity of lysozyme crystals. *Acta Crystallography*. 1998;**54**:581-590. DOI: 10.1107/s0108767398001986
- [20] Koshima H, Nagano M, Asahi T. Optical activity induced by helical arrangements of tryptamine and 4-chlorobenzoic acid in their cocrystal. *Journal of the American Chemical Society*. 2005;**127**:2455-2463. DOI: 10.1021/ja044472f
- [21] Herreros-Cedres J, Hernandez-Rodriguez C, Castro MP, Montoya MM, Rodriguez VL. Optical anisotropy of $\text{TGS}_x \cdot \text{TGSe}_{1-x}$ compounds. *Ferroelectrics*. 2007;**350**:22-28. DOI: 10.1080/00150190701369602
- [22] Kaminsky W. Experimental and phenomenological aspects of circular birefringence and related properties in transparent crystals. *Reports on Progress in Physics*. 2000;**63**:1575-1640. DOI: 10.1088/0034-4885/63/10/201
- [23] Shopa Y, Lutsiv-Shumskiy L, Serkiz R. Optical activity of the KDP group crystals. *Ferroelectrics*. 2005;**317**: 79-82. DOI: 10.1080/00150190590963480
- [24] Kaminsky W, Steininger S, Herreros-Cedres J, Glazer AM. Evidence of a circularly polarized light mode along the optic axis in *c*-cut $\text{NH}_4\text{H}_2\text{PO}_4$, induced by circular differential reflection and anomalous birefringence. *Journal of Physics: Condensed Matter*. 2010;**22**:095902. DOI: 10.1088/0953-8984/22/9/095902
- [25] Moxon JRL, Remshaw AR. The simultaneous measurement of optical activity and circular dichroism in birefringent linearly dichroic crystal sections. I. Introduction and description of the method. *Journal of Physics*. 1990; **2**:6807-6836. DOI: 10.1088/0953-8984/2/32/012
- [26] Kaminsky W, Glazer AM. Measurement of optical rotation in crystals. *Ferroelectrics*. 1996;**183**: 133-141. DOI: 10.1080/00150199608224099
- [27] Matsuki R, Asahi T, Kobayashi J, Asai H. Measurement of circular birefringence and circular dichroism of the single crystals of $\Lambda-(+)_589$ - and $\Delta-(-)_589$ -tris(ethylenediamine)cobalt (III) triiodide monohydrate by the extended HAUP method. *Chirality*.

2004;**16**:286-293. DOI: 10.1002/chir.20029

[28] Nakagawa K, Harper-Lovelady H, Tanaka Y, Tanaka M, Yamato M, Asahi T. A high-accuracy universal polarimeter study of optical anisotropy and optical activity in laminated collagen membranes. *Chemical Communications*. 2014;**50**:15086-15089. DOI: 10.1039/C3CC49328H

[29] Ishikawa K, Tanaka M, Suzuki T, Sekine A, Kawasaki T, Soai K, et al. Absolute chirality of the γ -polymorph of glycine: Correlation of the absolute structure with the optical rotation. *Chemical Communication*. 2012;**48**:6031-6033. DOI: 10.1039/C2CC30549F

[30] Koshima H, Matsuo R, Matsudomi M, Uemura Y, Shiro M. Light-driven bending crystals of salicylidenephenylethylamines in enantiomeric and racemate forms. *Crystal Growth & Design*. 2013;**13**:4330-4337. DOI: 10.1021/cg400675r

[31] Kitagawa D, Nishi H, Kobatake S. Photoinduced twisting of a photochromic diarylethene crystal. *Angewandte Chemie, International Edition*. 2013;**52**:9320-9322. DOI: 10.1002/anie.201304670

[32] Taniguchi T, Fujisawa J, Shiro M, Koshima H, Asahi T. Mechanical motion of chiral azobenzene crystals with twisting upon photoirradiation. *Chemistry - A European Journal*. 2016;**22**:7950-7958. DOI: 10.1002/chem.201505149

[33] Toll JS. Causality and the dispersion relation: Logical foundations. *Physics Review*. 1956;**104**:1760-1770. DOI: 10.1103/PhysRev.104.1760

[34] Kobayashi J, Uchino K, Asahi T. Optical properties of Rochelle salt.

Physical Review B. 1991;**43**:5706-5712. DOI: 10.1103/PhysRevB.43.5706

[35] Asahi T, Nakamura M, Kobayashi J, Toda F, Miyamoto H. Optical activity of oxo amide crystals. *Journal of the American Chemical Society*. 1997;**119**:3665-3669. DOI: 10.1021/ja9620189

[36] Raj JC, Dinakaran S, Krishnan S, Boaz MB, Robert R, Das JS. Studies on optical, mechanical and transport properties of NLO active *L*-alanine formate single crystal grown by modified Sankaranarayanan–Ramasamy (SR) method. *Optics Communication*. 2008;**281**:2285-2290. DOI: 10.1016/j.optcom.2007.12.019

[37] Simpson HJ Jr, Marsh RE. The crystal structure of *L*-alanine. *Acta Crystallography*. 1966;**20**:550-555. DOI: 10.1107/S0365110X66001221

[38] Lehmann MS, Koetzle TF, Hamilton WC. Precision neutron diffraction structure determination of protein and nucleic acid components. I. Crystal and molecular structure of the amino acid *L*-alanine. *Journal of the American Chemical Society*. 1972;**94**:2657-2660. DOI: 10.1021/ja00763a016

[39] Misoguti L, Valera AT, Nunes FD, Bagnato VS, Melo FEA, Mendes FJ, et al. Optical properties of *L*-alanine organic crystals. *Optical Materials*. 1996;**6**:147-152. DOI: 10.1016/0925-3467(96)00032-8

[40] Razzetti C, Ardoino M, Zanotti L, Zha M, Paorici C. Solution growth and characterisation of *L*-alanine single crystals. *Crystal Research and Technology*. 2002;**37**:456-465. DOI: 10.1002/1521-4079(200205)37:5<456::AID-CRAT456>3.0.CO;2-M

[41] Wojciechowski A, Ozga K, Reshak AH, Miedzinski R, Kityk IV,

- Berdowski J, et al. Photoinduced effects in *L*-alanine crystals. *Materials Letters*. 2010;**64**:1957-1959. DOI: 10.1016/j.matlet.2010.06.034
- [42] Bisker-Leib V, Doherty MF. Modeling crystal shape of polar organic materials: Applications to amino acids. *Crystal Growth & Design*. 2003;**3**: 221-237. DOI: 10.1021/cg025538q
- [43] Vijayan N, Rajasekaran S, Bhagavannarayana G, Ramesh BR, Gopalakrishnan R, Palanichamy M, et al. Growth and characterization of nonlinear optical amino acid single crystal: *L*-alanine. *Crystal Growth & Design*. 2006;**6**:2441-2445. DOI: 10.1021/cg049594y
- [44] Zhong H, Levine ZH, Allan DC, Wilkins JW. Optical activity of selenium: A nearly first-principles calculation. *Physical Review Letters*. 1992;**69**: 379-382. DOI: 10.1103/PhysRevLett.69.379
- [45] Lahiri P, Wiberg KB, Vaccaro PH, Caricato M, Crawford TD. Large solvation effect in the optical rotatory dispersion of norbornenone. *Angewandte Chemie*. 2014;**126**: 1410-1413. DOI: 10.1002/anie.201306339
- [46] Balduf T, Caricato M. Helical chains of diatomic molecules as a model for solid-state optical rotation. *Journal of Physical Chemistry C*. 2019;**123**: 4329-4340. DOI: 10.1021/acs.jpcc.8b12084
- [47] Rérat M, Kirtman B. First-principles calculation of the optical rotatory power of periodic systems: Application on α -quartz, tartaric acid crystal, and chiral (n,m)-carbon nanotubes. *Journal of Chemical Theory and Computation*. 2021;**17**:4063-4076. DOI: 10.1021/acs.jctc.1c00243
- [48] More M, Odou G, Lefebvre J. Structure determination of benzil in its two phases. *Acta Crystallography*. 1987;**43**:398-405. DOI: 10.1107/S0108768187097660
- [49] Chandrasekhar S. The rotatory dispersion of benzil. *Proceedings of the Indian Academy Science*. 1954;**39**:243-253. DOI: 10.1007/BF03047144
- [50] Chaudhuri NK, El-Sayed MA. Molecular origin of the optical rotatory dispersion of the benzil crystal. *The Journal of Chemical Physics*. 1967;**47**: 1133-1143. DOI: 10.1063/1.1711998
- [51] Jelley E. Application of grating microspectrograph to problem of identifying organic compounds. *Industrial and Engineering Chemistry, Analytical Edition*. 1941;**13**:196-203. DOI: 10.1021/i560091a022
- [52] Bryant WMD. Optical crystallographic studies with the polarizing microscope. IV. Axial dispersion with change of sign. Other dispersion measurements. *Journal of the American Chemical Society*. 1943;**65**:96-102. DOI: 10.1021/ja01241a031
- [53] Polavarapu PL. *Chiroptical Spectroscopy: Fundamentals and Applications*. 1st ed. Boca Raton: CRC Press; 2017. p. 448. DOI: 10.1201/9781315374888
- [54] Srebro-Hooper M, Autschbach J. Calculating natural optical activity of molecules from first principles. *Annual Review of Physical Chemistry*. 2017;**68**: 399-420. DOI: 10.1146/annurev-physchem-052516-044827
- [55] Kaminsky W, Weckert E, Kutzke H, Glazer AM, Klapper H. Non-linear optical properties and absolute structure of metastable 4-methyl benzophenone.

Crystal Materials. 2006;**221**:294-299.
DOI: 10.1524/zkri.2006.221.4.294

[56] Murphy VL, Kahr B. Hückel theory and optical activity. *Journal of the American Chemical Society*. 2015;**137**: 5177-5183. DOI: 10.1021/jacs.5b01763

[57] Murphy VL, Reyes A, Kahr B. Aromaticity and optical activity. *Journal of the American Chemical Society*. 2016; **138**:25-27. DOI: 10.1021/jacs.5b11138

[58] Molina P, Vasyliov V, Vllora EG, Shimamura K. CeF₃ and PrF₃ as UV-visible faraday rotators. *Optical Express*. 2011;**19**:11786-11791. DOI: 10.1364/OE.19.011786

[59] Vasyliov V, Vllora EG, Nakamura M, Sugahara Y, Shimamura K. UV-visible faraday rotators based on rare-earth fluoride single crystals: LiREF₄ (RE = Tb, Dy, Ho, Er and Yb), PrF₃ and CeF₃. *Optical Express*. 2012;**20**:14460-14470. DOI: 10.1364/OE.20.014460

[60] Vllora EG, Shimamura K, Plaza GR. Ultraviolet-visible optical isolators based on CeF₃ faraday rotator. *Journal of Applied Physics*. 2015;**117**:233101-233104. DOI: 10.1063/1.4922497

[61] Shinagawa K. Faraday and Kerr effects in ferromagnets. In: Sugano S, Kojima N, editors. *Magneto-optics*. 1st ed. Berlin: Springer; 2000. pp. 137-177

[62] Takanabe A, Koshima H, Asahi T. Fast-type high-accuracy universal polarimeter using charge-coupled device spectrometer. *AIP Advances*. 2017;**7**: 025209-025214. DOI: 10.1063/1.4977440

[63] Tanaka M, Yagi-Watanabe K, Kaneko F, Nakagawa K. First observation of natural circular dichroism spectra in the extreme ultraviolet region using a polarizing undulator-based

optical system and its polarization characteristics. *Journal of Synchrotron Radiation*. 2009;**16**:455-462. DOI: 10.1107/S0909049509012291